Negative ionic states of tin in the oxide superconductor Sr$_{3-x}$SnO revealed by Mössbauer spectroscopy

Atsutoshi Ikeda ⬤,[1,*] Shun Koibuchi,[1] Shinji Kitao,[2] Mohamed Oudah,[1,3] Shingo Yonezawa ⬤,[1]
Makoto Seto,[2] and Yoshiteru Maeno ⬤[1]

[1]*Department of Physics, Kyoto University, Kyoto 606-8502, Japan*
[2]*Institute for Integrated Radiation and Nuclear Science, Kyoto University, Osaka 590-0494, Japan*
[3]*Stewart Blusson Quantum Matter Institute, University of British Columbia, Vancouver, British Columbia, Canada V6T 1Z4*

We report the temperature variation of the ^{119}Sn-Mössbauer spectra of the antiperovskite (inverse perovskite) oxide superconductor Sr$_{3-x}$SnO. Both superconductive (Sr deficient) and nonsuperconductive (nearly stoichiometric) samples exhibit major γ-ray absorption with an isomer shift similar to that of Mg$_2$Sn. This fact shows that Sr$_{3-x}$SnO contains the metallic anion Sn^{4-}, which is rare, especially among oxides. In both samples, we observed another γ-ray absorption with a larger isomer shift, indicating that there is another ionic state of Sn with a higher oxidation number. The temperature dependence of the absorption intensities reveals that the Sn ions exhibiting larger isomer shifts have a lower energy of the local vibration. The larger isomer shift and lower vibration energy are consistent with the values estimated from the first-principles calculations for hypothetical structures with various Sr-deficiency arrangements. Therefore, we conclude that the additional γ-ray absorptions originate from the Sn atoms neighboring the Sr deficiency.

I. INTRODUCTION

Antiperovskite (inverse perovskite) oxides A_3BO (A: alkaline-earth elements, Eu, or Yb; B: group 14 elements) are the metal-rich counterpart of the ordinary perovskite oxides ABO$_3$, with inverted positions of the positive and negative ions [1]. In antiperovskite oxides, an oxygen ion is octahedrally coordinated by the metallic A^{2+} ions [Fig. 1(a)], while in ordinary perovskite oxides, a metal element is surrounded by O^{2-}. As a result of three A^{2+} ions in a unit cell, the oxidation number of B is forced to be 4− such as Sn^{4-} and Pb^{4-} to satisfy the charge neutrality as $(A^{2+})_3B^{4-}$O^{2-}. Novel physics and chemistry of such metallic anions, especially rare in oxides, have been motivating us to study this group of materials. Since Mössbauer spectroscopy is applicable to the Sn nucleus, microscopic characterization of such a Sn^{4-} state may unveil the nature of electronic states of antiperovskite oxides.

Due to the recent predictions of bulk Dirac cones [3,4] and a topological nature [5] in the vicinity of the Fermi energy, antiperovskite oxides are attracting a lot of attention [3–17]. After the initial theoretical predictions, the chemical and physical characters of antiperovskite oxides have been extensively investigated [6]. The metallic anion Sn^{4-} was experimentally observed in Sr$_3$SnO using Mössbauer spectroscopy at room temperature by some of the present authors [16]. The Dirac cone in the bulk band structure was confirmed in Ca$_3$PbO with angle-resolved photoemission spectroscopy (ARPES) [9], in Sr$_3$PbO with magnetotransport [13], and in Sr$_3$SnO with nuclear magnetic resonance (NMR) [15]. Furthermore,

thermoelectric properties of Ca$_3$SnO and Ca$_3$Pb$_{1-x}$Bi$_x$O are studied to make use of the multivalley band structure with six equivalent Dirac cones [7]. More recently, it was proposed that one can tune the size of the band inversion and mass of the Dirac cone via chemical substitution of A and B [10]. Thus, antiperovskite oxides are a good platform to study the Dirac and topological natures.

In 2016, some of the present authors discovered superconductivity in Sr$_{3-x}$SnO prepared with a nominal Sr deficiency of $x_0 = 0.5$ [8], the first superconductivity among the antiperovskite oxides. This material exhibits two superconducting transitions at $T_c \simeq 5$ and 0.8 K. Theoretical analyses indicate that the superconductivity in Sr$_{3-x}$SnO can be topological crystalline superconductivity with $j = 3/2$ pairing reflecting the topology of the electronic band structure in the normal state [8,14]. Band structure calculations [11] and NMR experiments [15] suggest heavy hole doping to Sn due to Sr deficiency. Indeed, Mössbauer spectra at room temperature revealed an additional ionic state of Sn having fewer electrons than Sn^{4-}, and its fraction increases with Sr deficiency [16]. However, the microscopic relation between the Sn states and Sr deficiency was not understood. In addition, the temperature evolution of the Mössbauer spectra has not been reported.

In this paper, we present the temperature dependence of the Sn-Mössbauer spectra for the nearly stoichiometric and Sr-deficient Sr$_{3-x}$SnO samples. Both samples exhibit two Sn states: Sn^{4-} characteristic of antiperovskite oxides and the other with a higher isomer shift particularly visible in the deficient sample. Detailed analyses of the temperature-dependent spectra show that the additional Sn state has a smaller number of electrons and lower energy of the local lattice vibrations. We also performed first-principles
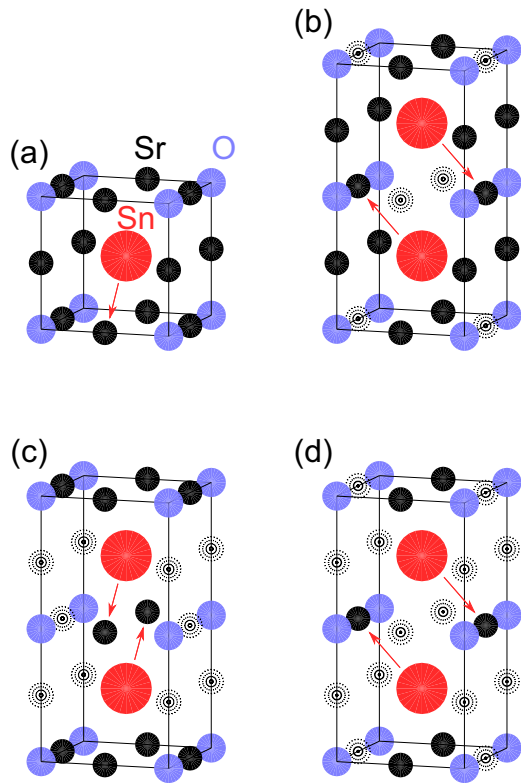
*a.ikeda@scphys.kyoto-u.ac.jp

FIG. 1. (a) Crystal structure of Sr_3SnO. In contrast to the common picture with the OSr_6 octahedron shown at the center, Sn (red sphere) is placed at the center of the unit cell in this picture. (b)–(d) Three hypothetical structures of highly Sr deficient antiperovskite oxides: (b) $Sr_4Sn_2O_2$, (c) $Sr_3Sn_2O_2$, and (d) $Sr_2Sn_2O_2$. The dotted spheres indicate the assumed positions of the Sr deficiency. The arrows indicate the direction of the atomic shift for the calculation of the force constants of Sn vibrations. The figures were prepared with the program VESTA [2].

calculations on various hypothetical Sr-deficient arrangements and successfully reproduced the experimental results. Therefore, we conclude that the additional Sn state originates from Sn atoms neighboring the Sr deficiency.

II. EXPERIMENT

A. Sample preparation

Polycrystalline samples of $Sr_{3-x}SnO$ were synthesized using the reaction $(3 - x_0)Sr + SnO \rightarrow Sr_{3-x}SnO + (x - x_0)Sr \uparrow$, where x_0 is the nominal Sr deficiency. Since Sr and $Sr_{3-x}SnO$ are highly air sensitive, reactants and products were handled in a glove box filled with argon. Sr (Sigma-Aldrich, 99.99%) and SnO (Sigma-Aldrich, 99.99%) were put in iron crucibles (Chiyoda Kogyo Seisakusho) with a molar ratio of $(3 - x_0):1$. The nearly stoichiometric (NS) sample was synthesized with the Sr-excess condition $x_0 = -0.5$ because preparation with $x_0 = 0$ results in a SrO impurity contained in the product. The crucible was sealed in a stainless-steel capsule (Fujikin, SUS316L pipe, $\phi 19.05 \times 1.65t \times 110$ mm sealed with Fujikin, V-LOK Cap, VUWJC-19.05) under 1 atm of argon at room temperature. The sealed capsule was heated to 1100 °C in 10.5 h, kept there for 50 h, and cooled down

to 800 °C in 6 h, using a muffle furnace (Denken Co. Ltd., KDF-S80). After subsequently being kept for 20 h at 800 °C, the capsule was cooled to room temperature in 8 h [6]. For the Sr-deficient (D) sample prepared with $x_0 = +0.5$, the crucible was sealed in a quartz tube under 0.3 atm of argon at room temperature. The tube was heated up to 850 °C over 3 h, kept there for 3 h, and quenched in water. Then the tube was heated again at 600 °C for 48 h, and was furnace-cooled.

For both NS ($x \simeq 0$) and D ($x \simeq 0.5$) samples, the actual Sr deficiency x was not measured. Since the Sr evaporation during the heating process was about 0.2% based on the difference of the mass before and after the reaction, we expect that the actual amount of deficiency is, in the D sample, close to its nominal value of 0.5. For the NS sample, the evaporation was only 6%, but the excess Sr seems to stick on the wall of the crucible, leading to a nearly stoichiometric value ($x \simeq 0$). For the samples prepared under conditions similar to the NS sample, energy dispersive x-ray spectroscopy (EDX) indicates that the Sr/Sn ratio is around 2.98 (i.e., $x = 0.02$). This result supports the idea that the actual x value of the NS sample is indeed small but also suggests that there is a certain amount of spontaneous Sr deficiency even in the NS sample. We note that Ca deficiency and corresponding hole doping are observed in a single crystal of Ca_3PbO by electron-probe microanalysis (EPMA) and ARPES [9]. For the samples prepared under conditions similar to the D sample, EDX shows a substantial spatial distribution of the Sr/Sn ratio, with the largest population at Sr/Sn = 2.5 (i.e., $x = 0.5$) [12].

B. Characterization

Powder x-ray diffraction (PXRD) patterns were collected with Cu $K\alpha$ radiation (wavelengths of 0.1540538 nm for $K\alpha_1$ and 0.1544324 nm for $K\alpha_2$) using a commercial diffractometer (Bruker AXS, D8 Advance) equipped with an array of 192 detectors. The diffracted x ray was integrated over 0.3 s for each angle, and the total measurement time was approximately 30 min for each sample. In order to prevent decomposition of the samples during the measurements, the samples were placed on a glass plate under argon atmosphere and were covered with a 12.5-μm-thick polyimide film (Du Pont-Toray Co. Ltd., Kapton 50H) fixed with vacuum grease (Dow Corning Toray, high-vacuum grease).

C. Magnetic properties

The size of the magnetic moment was measured using a commercial magnetometer with a superconducting quantum interference device (Quantum Design, MPMS-XL). The powder sample was put in a thin plastic capsule under argon atmosphere to avoid exposure to air.

D. Mössbauer spectroscopy

^{119m}Sn in the form of $CaSnO_3$ (Ritverc GmbH, 740 MBq) was used as the γ-ray source. The velocity of the source was calibrated using the absorptions of ^{57}Fe, and its origin was set to the isomer shift of $BaSnO_3$ at room temperature. A palladium film with a thickness of 75 μm was placed between the source and sample in order to stop the x-ray fluorescence of tin. After measurements of magnetization, the powder
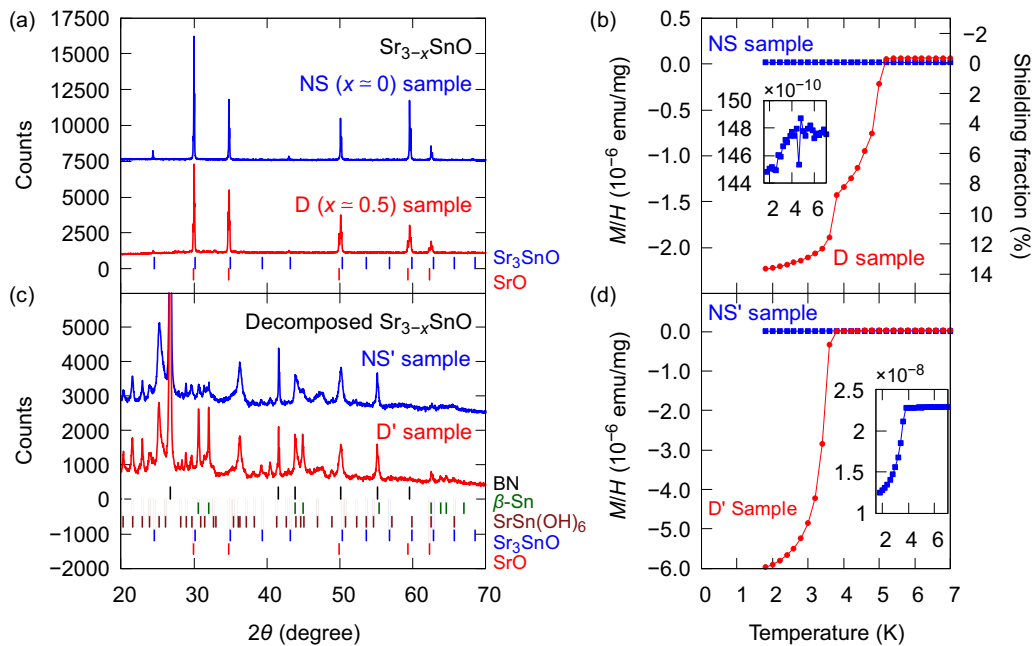
FIG. 2. (a) Powder x-ray diffraction patterns of the nearly stoichiometric (NS) sample (prepared with the Sr-excess condition of $x_0 = -0.5$) and Sr-deficient (D) sample (prepared with the Sr-deficient condition of $x_0 = +0.5$). The bars at the bottom indicate the peak positions of Sr_3SnO (PDF 01-084-0254) and SrO (PDF 01-075-6979). (b) Temperature dependence of the magnetization of $Sr_{3-x}SnO$ measured in a magnetic field of $\mu_0 H = 1$ mT under a zero-field-cooling (ZFC) condition. The inset shows a magnified view of the NS sample. (c) X-ray diffraction patterns after the NS and D samples were intentionally decomposed in air (NS′ and D′ samples, respectively). The bars at the bottom indicate the peak positions of BN (PDF 00-034-0421), β-Sn (PDF 01-086-2265), $SrSn(OH)_6$ (PDF 00-009-0086), Sr_3SnO, and SrO. (d) Temperature dependence of the magnetization of the decomposed NS′ and D′ samples measured in a magnetic field of $\mu_0 H = 2$ mT and under a ZFC condition. The inset shows a magnified view of the NS′ sample. When evaluating magnetization, the mass of the mixed BN and polyethylene powder was subtracted.

(around 40 mg) was taken out from the capsule and mixed with boron nitride (Kishida Chemical, 99.5%; approximately 70 mg) and polyethylene (Beckman RIIC, polyethylene powder for IR spectroscopy; approximately 8 mg) powders under nitrogen atmosphere in order to improve the spatial homogeneity of the sample. Then the sample was pressed into a pellet with a diameter of 10 mm and sealed in multiple layers of polyethylene bags with a thickness of 0.1 mm in order to avoid direct contact with air. All the measurements, from room temperature to below 3 K, were carried out inside a ^{4}He cryostat (Janis Research, ST-400). Typical measurement time was 12 h at each temperature.

E. First-principles calculation

To analyze the Mössbauer spectra of $Sr_{3-x}SnO$, we performed first-principles calculations. Here, we calculated electronic densities of various Sn-based materials, including $Sr_{3-x}SnO$, in order to deduce the relation between the electronic density and the isomer shift. The density of electrons at the tin nucleus position was calculated by the full-potential linearized augmented plane-wave plus local orbitals method using the WIEN2K package [18]. The Perdew-Burke-Ernzerhof generalized gradient approximation [19] was selected as the exchange-correlation functional. The spin-orbit coupling was taken into account. We chose the muffin-tin radius (RMT) of each atom to be $RMT_{Sr} = 2.41$, $RMT_{Sn} = 2.5$, and $RMT_O = 2.41$ in units of the Bohr radius a_B. We set the plane-wave cutoff as $RK_{max} = 8$, the highest angular momentum

as $l_{max} = 10$, the maximum magnitude of the largest vector in charge density Fourier expansion as $G_{max} = 18$, and the separation energy between the valence and core states as -7.0 Ry [20]. Only when estimating the energy of the local lattice vibrations in the hypothetical superstructure "$Sr_2Sn_2O_2$" did we use the separation energy of -6.0 Ry in order to avoid a technical problem. The Inorganic Crystal Structure Database numbers of the experimentally reported structures and the sizes of the k mesh used for calculations were 78894 and $12 \times 12 \times 12$ for SnF_4, 239582 and $12 \times 12 \times 12$ for $BaSnO_3$, 411242 and $10 \times 15 \times 10$ for $SnCl_4$, 43594 and $14 \times 14 \times 7$ for $SnSe_2$, 642850 and $12 \times 12 \times 12$ for Mg_2Sn, 40038 and $12 \times 12 \times 12$ for β-Sn, 186650 and $6 \times 17 \times 16$ for SnSe, and 15452 and $10 \times 18 \times 8$ for $SnCl_2$. The calculated electronic densities of these compounds were compared with the experimentally observed isomer shifts [21,22]. For Sr_3SnO, we used the structure reported by Nuss *et al.* [6] and a k mesh of $12 \times 12 \times 12$. For strontium-deficient $Sr_{3-x}SnO$, hypothetical structures based on Sr_3SnO ("$Sr_4Sn_2O_2$," "$Sr_3Sn_2O_2$," and "$Sr_2Sn_2O_2$"; see Fig. 1; k mesh of $12 \times 12 \times 6$) were assumed.

III. RESULTS

A. Sample characterization

First, we show PXRD patterns of our samples in Fig. 2(a). The NS ($x \simeq 0$) sample exhibits no detectable impurity peaks. All the peaks were indexed with space group $Pm\bar{3}m$ (No. 221,
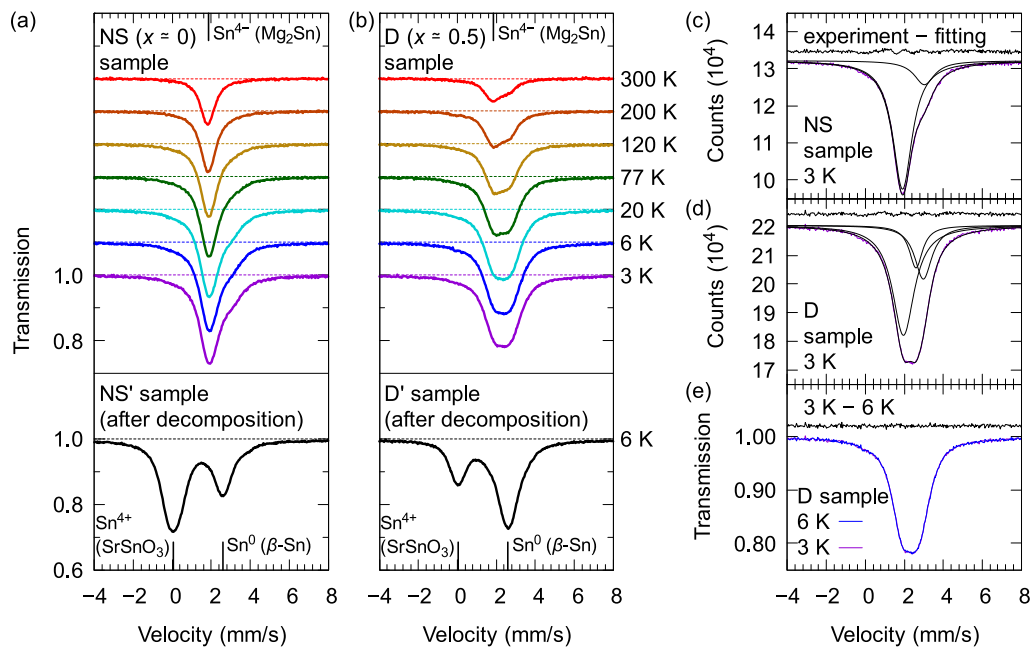
FIG. 3. Temperature dependence of the ^{119}Sn-Mössbauer spectra of (a) the nearly stoichiometric (NS) and (b) Sr-deficient (D) $Sr_{3-x}SnO$ samples. All spectra have the same scale, and each spectrum is shifted upward by 0.1 so that the change in the peak shape is more visible. The dashed line for each spectrum indicates the transmission of 100%. For each panel, the bottom spectrum was obtained at 6 K after intentional decomposition in air (NS′ and D′ samples). The vertical lines at 1.87, 0.05, and 2.60 mm/s indicate the isomer shifts of Mg_2Sn at 300 K [21], $SrSnO_3$ at 100 K [23], and β-Sn at 4.2 K [24], respectively, representing Sn^{4-}, Sn^{4+}, and Sn^0 ionic states. (c) and (d) Results of Lorentzian fittings of the spectra of the NS and D samples at 3 K for quantitative analysis of the isomer shifts and absorption intensities. The sum of the Lorentzians reasonably reproduces the experimental spectra. (e) Comparison of the spectra above (6 K, blue curve) and below (3 K, purple curve) the superconducting transition temperature of the D sample. The two spectra almost overlap each other, and the difference between the two spectra (shifted upward) is a straight line within the noise level.

O_h^1) and the lattice parameter $a = 0.513767(6)$ nm of Sr_3SnO [6]. For the pattern of the D ($x \simeq 0.5$) sample, the peaks were indexed with $a = 0.51246(5)$ nm except for the left shoulder peaks originating from insulating SrO, which also has a cubic crystalline structure (space group $Fm\bar{3}m$, No. 225, O_h^5) with a slightly larger lattice parameter $a = 0.51463(5)$ nm. Figure 2(b) shows the temperature dependence of the magnetizations of these samples. The NS sample does not show superconductivity of $Sr_{3-x}SnO$. As shown in the inset, the magnetization very slightly decreases below 3.7 K, which originates from the superconductivity of tin impurity that was not detected with PXRD. In contrast, the D sample shows the Meissner effect below 5 K, originating from the superconductivity of $Sr_{3-x}SnO$ [8]. The shoulderlike structure at 3.7 K is attributable to the superconductivity of the Sn impurity. Comparing magnetization data above and below 3.7 K, we estimate the diamagnetism due to superconductivity of β-Sn as 0.58×10^{-6} emu/mg, which corresponds to 5.4 wt % or 14 mol % of the β-Sn inclusion.

After the magnetization and Mössbauer measurements, both NS ($x \simeq 0$) and D ($x \simeq 0.5$) samples were intentionally decomposed in air for a few days (hereafter referred to as NS′ and D′ samples), and their PXRD patterns and magnetizations were measured again. The large peak at $2\theta = 27°$ as well as several others in the PXRD pattern [Fig. 2(c)] originates from boron nitride mixed for the Mössbauer experiments. The decomposed samples mainly consist of $SrSn(OH)_6$. In addition, the D′ sample exhibits clear peaks from β-Sn, whereas the

peaks from β-Sn in the NS′ sample are rather faint. As shown in Fig. 2(d), the D′ sample exhibits strong diamagnetism below 3.7 K due to the superconductivity of Sn. The NS′ sample exhibits much weaker diamagnetism, as shown in the inset.

B. Mössbauer spectroscopy

^{119}Sn-Mössbauer spectra of $Sr_{3-x}SnO$ samples at various temperatures are presented in Fig. 3. Both NS ($x \simeq 0$) and D ($x \simeq 0.5$) samples strongly absorb the γ ray around the isomer shift of $+1.9$ mm/s. This shift is very close to that of Mg_2Sn ($+1.87$ mm/s at 300 K [21]), in which the Sn^{4-} state is anticipated. In addition, minor γ-ray absorptions are observed at slightly higher isomer shifts, as evidenced by the shoulderlike structure in the spectra.

To analyze the data more quantitatively, we fitted the spectra with multiple Lorentzian functions and evaluated their isomer shifts and integrated peak intensities. For the NS sample, we used two Lorentzians to fit the major and minor absorptions [Fig. 3(c)]. We confirmed that the minor absorption is not due to the β-Sn impurity because the observed isomer shift of $+3.03(2)$ mm/s at the lowest temperature is clearly different from the reported isomer shift of β-Sn (2.60 mm/s at 4.2 K [24]). For the D sample, we added one extra Lorentzian to take into account the contribution of the β-Sn impurity [Fig. 3(d)]. The isomer shift of the Sn impurity is fixed to the reported value. The intensity is also fixed so that the integrated peak area becomes 14% of the

total area at the lowest temperature as calculated from the temperature dependence of the magnetization [Fig. 2(b)]. The fitting well explains the data, and the isomer shift of the minor absorption at 3 K was evaluated to be +2.973(11) mm/s, which is again distinct from the isomer shift of β-Sn. Thus, this minor absorption of the NS and D samples should be intrinsic to $Sr_{3-x}SnO$.

From the integrated intensity of the spectra at the lowest temperature, the fractions of the tin atoms related to these minor absorptions are estimated to be 16.4(9)% in the NS ($x \simeq 0$) sample and 27.9(12)% in the D ($x \simeq 0.5$) sample. Since the intensity of the minor absorption increases with the strontium deficiency, the tin atoms near the Sr deficiency are ascribable to the origin of this minor absorption.

In order to estimate the amount of the Sr deficiency x, let us assume for simplicity that the $Z = 12$ Sr atoms surrounding a Sn atom can be extracted independently. In this case, the probability that a Sn atom does not have any neighboring Sr deficiency is $(1 - x/3)^Z$. Then, the relative intensity of the minor absorption, originating from Sn atoms next to Sr deficiencies, is given by $1 - (1 - x/3)^Z$. Assuming that the observed 16% minor absorption in the NS ($x \simeq 0$) sample is explained by this formula, we obtain $x = 0.04$. This estimated value of x is consistent with the results of EDX, yielding $x = 0.02$, as explained above. This good agreement confirms the scenario that minute spontaneous Sr deficiency leads to a minor absorption with relatively strong intensity. A similar amount of the Ca deficiency is reported by EPMA in a single crystal of Ca_3PbO [9]. Such an amount of deficiency should be insufficient to trigger superconductivity. For the D ($x \simeq 0.5$) sample, the same assumption leads to the equation $1 - (1 - x/3)^Z = 0.28$, whose solution is $x \simeq 0.08$. This value is substantially smaller than the nominal Sr deficiency of $x_0 = 0.5$, probably because the simple assumption of independent deficiency distribution is no longer valid for such a large value of x. This implies that the Sr deficiencies tend to cluster each other, rather than distributing just randomly, when the amount of deficiency becomes larger.

Let us discuss the origin of the minor absorption in more detail. Generally speaking, the isomer shift reflects the density of electrons at the nucleus position. This is because the nuclei in the ground and excited states have slightly different effective radii. For the Sn nucleus, the excited nucleus has a larger radius than the ground-state one. Thus, if the density of the electrons at the nucleus site is larger, the energy difference between the excited and ground states becomes larger because the excited nucleus feels less Coulomb attraction from the surrounding electrons. As a consequence, a larger density of electrons results in a larger isomer shift [25]. Thus, more s electrons lead to a more positive isomer shift because s electrons have a nonzero probability amplitude at the nucleus position. In contrast, p or d electrons result in a negative and smaller shift via the screening effect. Therefore, it is expected that the minor absorption with a larger isomer shift will originate from tin ions with fewer p electrons than Sn^{4-}, or, in other words, the hole-doped ionic states due to strontium deficiency.

In order to confirm that the minor absorptions do not originate from partial decomposition of the samples, we measured the Mössbauer spectra of the intentionally decomposed samples (NS′ and D′ samples). After the decomposition, the γ-ray absorptions are located at 0.0–0.1 and 2.6 mm/s at 6 K. These absorptions are very similar to those of $SrSnO_3$ (0.05 mm/s at 100 K [23]) and β-Sn (2.60 mm/s at 4.2 K [24]). This result indicates that $Sr_{3-x}SnO$ decomposes into β-Sn and a certain material containing a Sn^{4+} ion [presumably $SrSn(OH)_6$, as seen in the PXRD pattern] and possibly some other compounds without tin. If the samples had decomposed during the setup of the Mössbauer experiments, we would have observed the absorption of Sn^{4+}. However, the actual spectra of the pristine samples do not show any absorption at around 0 mm/s. Therefore, we can exclude the possibility that the minor absorptions originate from partial decomposition.

To examine the temperature evolution of the Mössbauer effect, we plot the temperature dependence of the isomer shift and integrated intensity in Fig. 4. The isomer shifts of the major absorptions are almost equal in the NS ($x \simeq 0$) and D ($x \simeq 0.5$) samples. This fact suggests that the strontium deficiency affects the density of electrons at the nucleus position very locally such that a major fraction of the tin atoms remains unchanged from Sn^{4-} even in the D sample.

From the temperature dependence of the spectra, we can calculate the energy of the local vibration of a Sn atom. Since the thermal vibration of an atom changes the relative energy of the γ ray by the Doppler effect, the intensity of the resonant absorption is suppressed at high temperature. Therefore, the temperature dependence of the intensity reflects the thermal vibration and provides information on the binding strength between the atom and the lattice. The observed temperature dependence of the integrated intensity is plotted in Fig. 4(b). Assuming that the intensity is proportional to the recoil-free fraction f, the data were fitted with the Debye model [26]:

$$f = \exp\left(-\frac{(2\pi)^2 \langle r^2 \rangle_D}{\lambda^2}\right), \tag{1}$$

$$\langle r^2 \rangle_D = \frac{3\hbar^2}{Mk_B\Theta_D}\left[\frac{1}{4} + \left(\frac{T}{\Theta_D}\right)^2 \int_0^{(\Theta_D/T)} \frac{y\,dy}{e^y - 1}\right], \tag{2}$$

where $\langle r^2 \rangle_D$ is the mean-square displacement in the Debye solid, $\lambda = 0.51933$ nm is the wavelength of the γ ray, $\hbar$ is the reduced Planck constant, M is the mass of a ^{119}Sn atom, k_B is the Boltzmann constant, and Θ_D is the effective Debye temperature (or Mössbauer temperature) characterizing the vibrations of the Sn atoms. As shown in Fig. 4(b), the fitting reproduces well the temperature dependences of all absorptions. The extracted Θ_D, as well as the isomer shifts, are summarized in Table I. Comparing Θ_D of all absorptions, there is a tendency that Θ_D decreases as the isomer shift increases. This tendency can be again understood as the effect of the local strontium deficiency: The higher local strontium deficiency leads to the lower density of the p electrons at the tin atoms and also to weaker binding of the atoms to the lattice.

We also tried fitting with the Einstein model [26]:

$$\langle r^2 \rangle_E = \frac{\hbar^2}{2Mk_B\Theta_E}\coth\left(\frac{\Theta_E}{2T}\right), \tag{3}$$
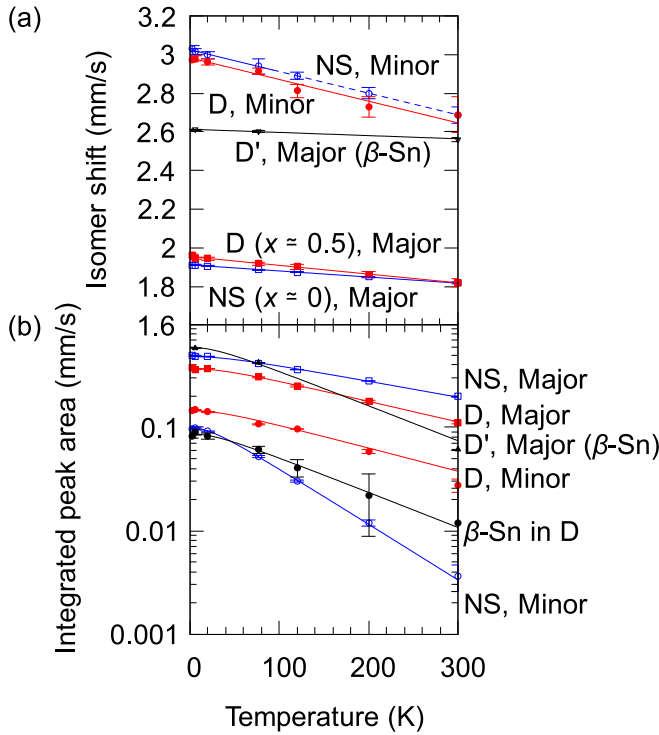
FIG. 4. Temperature dependence of (a) the isomer shifts and (b) integrated peak areas obtained by fitting the spectra with multiple Lorentzians. For the contribution from the β-Sn impurity in the D ($x \simeq 0.5$) sample, we assumed that the integrated peak area exhibits the same temperature dependence as that of β-Sn contained in the D$'$ sample. For the NS ($x \simeq 0$) sample and at temperatures above 100 K, the double-Lorentzian fitting with six independent parameters (two sets of the peak position, intensity, and width) was not successful because of the too small contribution from the minor absorption. Thus, we estimated the isomer shift of the minor absorption by the following way and fixed the shift in the fitting (i.e., now we used five independent parameters). First, we assumed that the isomer shift of the minor absorption exhibits a linear temperature dependence. Then the slope of the temperature dependence is assumed to be the same as that of the D sample. Under these assumptions, we extrapolated the data of the NS sample below 100 K to higher temperatures to estimate the isomer shift at 120, 200, and 300 K, as indicated with the blue dashed line in (a).

where Θ_E is the effective Einstein temperature. The fitting is as good as that with the Debye model but has a slightly larger residual sum of squares. We found that $\sqrt{3}\Theta_E$ gave almost the same temperature as Θ_D. This agrees with the theoretical relation $\sqrt{3}\Theta_E = \Theta_D$ deduced under the assumption of the same mean-square displacements in the Einstein and Debye solids at high temperature: $\langle r^2 \rangle_E = \langle r^2 \rangle_D$ [26].

Before closing this section, we would like to comment on the Mössbauer spectrum in the superconducting state. We did not observe any clear difference in the spectra across the superconducting transition, as shown in Fig. 3(e). Since superconductivity does not cause a large change in the electronic density at the nucleus, the superconducting transition is, in most cases, difficult to observe with Mössbauer spectroscopy in terms of the isomer shift [27] and the recoil-free fraction [28]. To observe superconductivity in Sr$_{3-x}$SnO in the

TABLE I. Isomer shifts (IS) at 300 K and effective Debye temperatures Θ_D characterizing the vibration of the Sn atoms, obtained from experiments and calculations. The accuracy of the experimental isomer shifts is expected to be about 0.01 mm/s. The error of the experimental values is defined as the standard error of double-Lorentzian fitting unless explicitly explained in the footnote. As for the major absorption of the NS ($x \simeq 0$) sample, the standard error of the fitting is smaller than the expected accuracy. The accuracy of the calculated isomer shifts is around 0.2 mm/s.

Absorption	IS (mm/s)	Θ_D (K)
Major [NS ($x \simeq 0$) sample]	1.82	222(3)
Major [D ($x \simeq 0.5$) sample]	1.82(2)	196(2)
Sr$_3$SnO (calculation)	1.7	186.5(8)
Minor (NS sample)	2.69(4)[a]	119.8(6)
Minor (D sample)	2.69(9)	185(7)
β-Sn in the D$'$ sample	2.56(1)	151(8)
Sr$_2$Sn$_2$O$_2$ (calculation)	3.1	97(3)
Sr$_3$Sn$_2$O$_2$ (calculation)	2.8	148.5(18)
Sr$_4$Sn$_4$O$_4$ (calculation)	2.4	148.3(13)

[a]Evaluated by linear extrapolation from the data at low temperatures (not by the Lorentzian fitting): Extrapolation error is presented.

Mössbauer spectroscopy, we need to enhance the resolution as well as to use samples with a larger superconducting volume fraction. These are the focus of future works.

C. Comparison with first-principles calculation

The relation between the experimental isomer shift (IS) at room temperature [21,22] and calculated electronic density at the Sn-nucleus position for various compounds is summarized in Fig. 5. We find an anticipated linear relation [25]: IS $= \alpha \, \Delta\rho + \beta$, with $\alpha = 0.071(2)a_B^3$ mm/s and $\beta = -0.03(6)$ mm/s, where $\Delta\rho$ is the electronic density with respect to that of BaSnO$_3$ ($262122.8a_B^{-3}$ in our calculation). The coefficient α is smaller than the previously reported values by 10%–20% [29,30]. This discrepancy should originate from the difference in the calculation methods.

From this relation, the isomer shift can be estimated from the electron-density calculation with an accuracy of around 0.2 mm/s. The calculated isomer shifts of Sr$_{3-x}$SnO are listed in Table I. The isomer shift of the major absorption agrees with the calculation for Sr$_3$SnO. For the minor absorption, we calculated the density of electrons assuming various hypothetical arrangements of the Sr deficiency and found that the calculated isomer shift of "Sr$_3$Sn$_2$O$_2$" [Fig. 1(c)] reasonably reproduces the observed values of the minor absorptions.

The force constant k between the Sn atom and the surrounding lattice in Sr$_{3-x}$SnO was estimated from the change in the total energy due to the virtual displacement of the Sn atom toward the nearest-neighboring strontium atom (see the arrows in Fig. 1): $\Delta E = k(r - r_0)^2/2 + E_0$, where ΔE is the change in energy, r is the displacement of the Sn atom, r_0 is the stable atomic position along the direction of displacement, and E_0 is the minimum energy corresponding to $r = r_0$. The effective Debye temperature was then calculated by $\Theta_D = \sqrt{3}\Theta_E = \sqrt{3}(\hbar/k_B)\sqrt{k/M}$ [26]. Figure 6 shows the change in energy and results of the fitting. The extracted effective Debye temperatures are listed in Table I. The overall trend
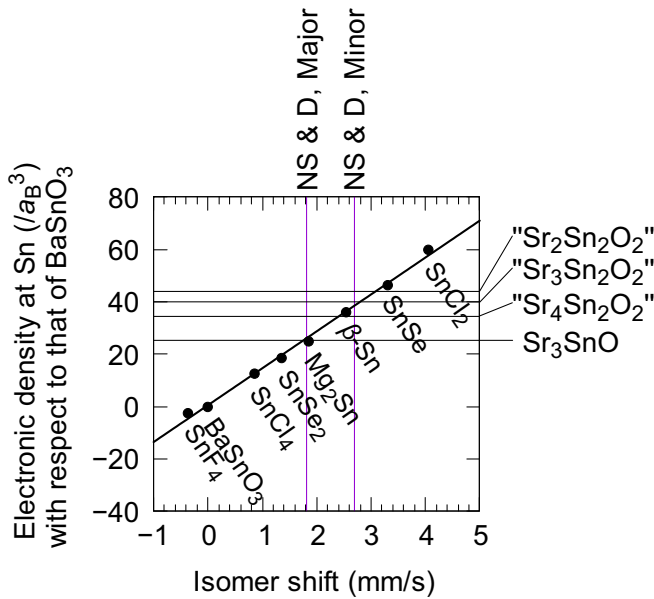
FIG. 5. Calculated electronic density versus experimental isomer shifts at room temperature [21,22]. The thick solid line shows the result of the linear fitting to the data points. The thin horizontal and vertical lines indicate the calculated electronic densities at the Sn nucleus of various Sr_3SnO-based structures and observed isomer shifts of the NS ($x \simeq 0$) and D ($x \simeq 0.5$) samples, respectively.

of the decreasing Θ_D with the increase of the isomer shift is reproduced in the calculation. The calculated Θ_D of Sr_3SnO and the experimental Θ_D of the major absorption of the NS ($x \simeq 0$) sample differ by 16%. For the minor absorptions, the calculated Θ_D of "$Sr_2Sn_2O_2$" and "$Sr_3Sn_2O_2$" match the experimental Θ_D of the minor absorptions in the NS and
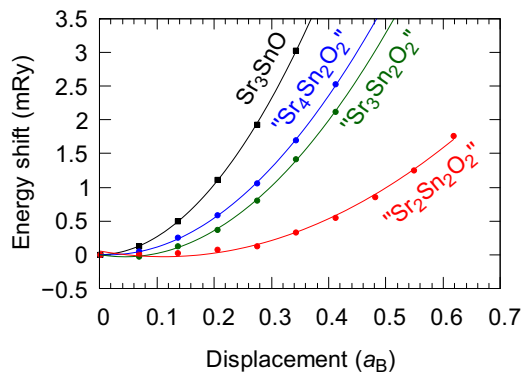
FIG. 6. Total energies of Sr_3SnO, $Sr_4Sn_4O_4$, $Sr_3Sn_2O_2$, and $Sr_2Sn_2O_2$ as functions of the displacement of the Sn atom calculated using the WIEN2K program. More Sr-deficient structures exhibit smaller changes in the total energy with displacement of the Sn atom, meaning that these materials have lower force constants of the lattice. In the highly deficient structures, the relative energy goes negative once with a small displacement. This means that the original atomic position (zero displacement) is unstable. Therefore, we fitted the data with the function $\Delta E = k(r - r_0)^2/2 + E_0$ with the stable atomic position r_0, the force constant k, and the minimum energy E_0 as fitting parameters. The results of the fittings are shown with the solid curves.
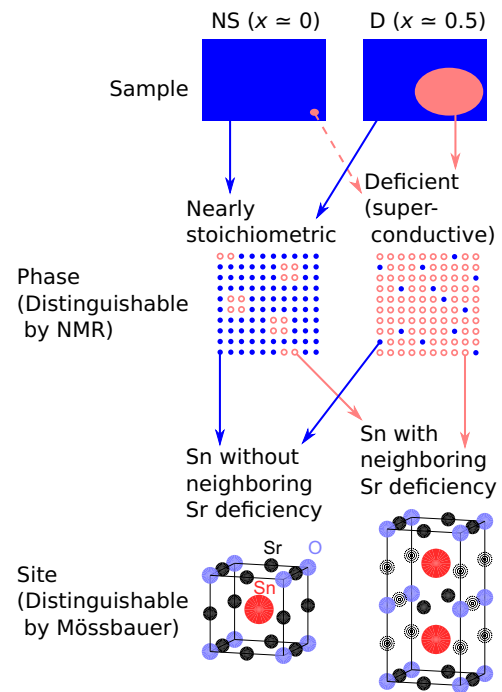

FIG. 7. Schematic illustration of the phase and site splittings. The NS sample is dominated by the nearly stoichiometric phase (blue), possibly with a separated inclusion of the deficient phase (red). In contrast, the D sample contains about 10% of the deficient superconductive phase. The nearly stoichiometric phase consists mostly of the Sn atom without the neighboring deficiency of Sr (blue solid circles), while the superconductive phase is composed mainly of the Sn atom with neighboring deficiency (red open circles).

D ($x \simeq 0.5$) samples, respectively, with accuracies similar to those for the major absorption.

These good agreements between the calculated and experimental values confirm that the origins of the major and minor absorptions are the tin atoms without and with the neighboring strontium deficiency, respectively. We note that the local deficiency seems to be more in the NS ($x \simeq 0$) sample than in the D ($x \simeq 0.5$) sample judging from the estimation of Θ_D of the minor absorptions. This may be due to the slow cooling at the end of the synthesis of the NS sample; the stoichiometric Sr_3SnO solidifies first, and $Sr_{3-x}SnO$ with a large deficiency is formed later as a minority phase. In the case of the D sample, in contrast, relatively rapid cooling leads to a large amount of deficient $Sr_{3-x}SnO$ but with relatively dilute deficiency.

D. Comparison with NMR

We comment that the phase splitting into the nearly stoichiometric and deficient compounds was suggested in a previous study of magnetization [16] and indeed observed with NMR [15]. Since NMR probes properties of the conduction electrons even though it measures the Zeeman energy of the Sn nucleus, the splitting in the NMR spectrum suggests that one sample consists of two materials ("phases") with distinct stoichiometries, as shown in Fig. 7. Similar phase splitting must exist also in the current samples, judging from the shielding fraction lower than 100%. On the other

hand, Mössbauer spectroscopy detects the local information at the nucleus position, and thus, the two absorptions may originate from two different sites in each phase. Since highly deficient phases such as $Sr_3Sn_2O_2$ and $Sr_2Sn_2O_2$ will be chemically unstable, it is unlikely that one sample separates into the two phases Sr_3SnO and $Sr_3Sn_2O_2$. Thus, we conclude that the minor absorption reflects the local Sr deficiency in each of the phases contained in $Sr_{3-x}SnO$ with $x \simeq 0$ in the NS sample and with $x \simeq 0.5$ in the D sample.

To sum up, we consider that our samples contain nearly stoichiometric and deficient phases, as depicted in Fig. 7. Each of these phases contains Sn sites with and without neighboring Sr deficiencies. Previous NMR measurements observed the phase splitting but could not detect such site splitting within each phase. In contrast, Mössbauer spectroscopy detects the difference in the Sn sites with and without neighboring Sr deficiency but hardly distinguishes similar sites in different phases.

The present results confirm the Sn^{4-} state and thus the validity of the band structure calculations. In this sense, these results are consistent with the NMR experiments observing $1/T_1$ attributable to the Dirac dispersion [15]. Furthermore, since the large amount of the Sr deficiency to "$Sr_3Sn_2O_2$" or "$Sr_2Sn_2O_2$" leads to heavy hole doping, the deficient phase containing a large portion of such Sn sites with neighboring Sr deficiency would exhibit metallic $1/T_1$, as indeed observed in the NMR measurements.

IV. CONCLUSION

By combining the Mössbauer spectroscopy and first-principles calculations, we confirmed the Sn^{4-} state in the antiperovskite oxide $Sr_{3-x}SnO$. Furthermore, we identified the origin of the minor absorption to be the Sn atoms with the neighboring Sr deficiency. From the effective energy of the local lattice vibrations, we infer that the local Sr deficiency is more in the nonsuperconductive sample, implying that the moderate deficiency between "$Sr_4Sn_2O_2$" and "$Sr_3Sn_2O_2$" is needed for superconductivity in $Sr_{3-x}SnO$. As a future experiment, measurements of the Sr-Sr distance using a pair-distribution function will further clarify the local environment of the Sr deficiency. We hope that microscopic understanding of the novel ionic states will lead to new chemistry and physics of metallic anions and will also contribute to development of Mössbauer spectroscopy.

[1] A. Widera and H. Schafer, Übergangsformen zwischen zintl-phasen und echten salzen: Die verbindungen A_3BO (mit $A =$ Ca, Sr, Ba und $B =$ Sn, Pb), Mater. Res. Bull. **15**, 1805 (1980).

[2] K. Momma and F. Izumi, VESTA 3 for three-dimensional visualization of crystal, volumetric and morphology data, J. Appl. Crystallogr. **44**, 1272 (2011).

[3] T. Kariyado and M. Ogata, Three-Dimensional Dirac Electrons at the Fermi Energy in Cubic Inverse Perovskites: Ca_3PbO and Its Family, J. Phys. Soc. Jpn. **80**, 083704 (2011).

[4] T. Kariyado and M. Ogata, Low-Energy Effective Hamiltonian and the Surface States of Ca_3PbO, J. Phys. Soc. Jpn. **81**, 064701 (2012).

[5] T. H. Hsieh, J. Liu, and L. Fu, Topological crystalline insulators and Dirac octets in antiperovskites, Phys. Rev. B **90**, 081112(R) (2014).

[6] J. Nuss, C. Mühle, K. Hayama, V. Abdolazimi, and H. Takagi, Tilting structures in *inverse* perovskites, M_3TtO ($M =$ Ca, Sr, Ba, Eu; $Tt =$ Si, Ge, Sn, Pb), Acta Crystallogr., Sect. B **71**, 300 (2015).

[7] Y. Okamoto, A. Sakamaki, and K. Takenaka, Thermoelectric properties of antiperovskite calcium oxides Ca_3PbO and Ca_3SnO, J. Appl. Phys. **119**, 205106 (2016).

[8] M. Oudah, A. Ikeda, J. N. Hausmann, S. Yonezawa, T. Fukumoto, S. Kobayashi, M. Sato, and Y. Maeno, Superconductivity in the antiperovskite Dirac-metal oxide $Sr_{3-x}SnO$, Nat. Commun. **7**, 13617 (2016).

[9] Y. Obata, R. Yukawa, K. Horiba, H. Kumigashira, Y. Toda, S. Matsuishi, and H. Hosono, ARPES studies of the inverse perovskite Ca_3PbO: Experimental confirmation of a candidate 3D Dirac fermion system, Phys. Rev. B **96**, 155109 (2017).

[10] T. Kariyado and M. Ogata, Evolution of band topology by competing band overlap and spin-orbit coupling: Twin Dirac cones in Ba_3SnO as a prototype, Phys. Rev. Mater. **1**, 061201 (2017).

[11] A. Ikeda, T. Fukumoto, M. Oudah, J. N. Hausmann, S. Yonezawa, S. Kobayashi, M. Sato, C. Tassel, F. Takeiri, H. Takatsu, H. Kageyama, and Y. Maeno, Theoretical band structure of the superconducting antiperovskite oxide $Sr_{3-x}SnO$, Physica B Condens. Matter **536**, 752 (2018).

[12] J. N. Hausmann, M. Oudah, A. Ikeda, S. Yonezawa, and Y. Maeno, Controlled synthesis of the antiperovskite oxide superconductor $Sr_{3-x}SnO$, Supercond. Sci. Technol. **31**, 055012 (2018).

[13] S. Suetsugu, K. Hayama, A. W. Rost, J. Nuss, C. Mühle, J. Kim, K. Kitagawa, and H. Takagi, Magnetotransport in Sr_3PbO antiperovskite, Phys. Rev. B **98**, 115203 (2018).

[14] T. Kawakami, T. Okamura, S. Kobayashi, and M. Sato, Topological Crystalline Materials of $J = 3/2$ Electrons: Antiperovskites, Dirac Points, and High Winding Topological Superconductivity, Phys. Rev. X **8**, 041026 (2018).

[15] S. Kitagawa, K. Ishida, M. Oudah, J. N. Hausmann, A. Ikeda, S. Yonezawa, and Y. Maeno, Normal-state properties of the

antiperovskite oxide $Sr_{3-x}SnO$ revealed by ^{119}Sn-NMR, Phys. Rev. B **98**, 100503(R) (2018).

[16] M. Oudah, J. N. Hausmann, S. Kitao, A. Ikeda, S. Yonezawa, M. Seto, and Y. Maeno, Evolution of Superconductivity with Sr-Deficiency in Antiperovskite Oxide $Sr_{3-x}SnO$, Sci. Rep. **9**, 1831 (2019).

[17] T. Kariyado, Counting pseudo Landau levels in spatially modulated Dirac systems, J. Phys. Soc. Jpn. **88**, 083701 (2019).

[18] P. Blaha, K. Schwarz, G. Madsen, D. Kvasnicka, and J. Luitz, *WIEN2K, an Augmented Plane Wave Plus Local Orbital Program for Calculating Crystal Properties* (Vienna University of Technology Institute of Materials Chemistry, Vienna, 2016).

[19] J. P. Perdew, K. Burke, and M. Ernzerhof, Generalized Gradient Approximation Made Simple, Phys. Rev. Lett. **77**, 3865 (1996).

[20] J. Batool, S. M. Alay-e Abbas, A. Ali, K. Mahmood, S. Akhtar, and N. Amin, The role of intrinsic vacancy defects in the electronic and magnetic properties of Sr_3SnO: A first-principles study, RSC Adv. **7**, 6880 (2017).

[21] J. G. Stevens, Isomer shift reference scales, Hyperfine Interact. **13**, 221 (1983).

[22] L. Fournès, J. Grannec, Y. Potin, and P. Hagenmuller, Mössbauer resonance investigations on the $SnF_2 \cdot SnF_4$ system, Solid State Commun. **59**, 833 (1986).

[23] P. Z. Hien, V. S. Shpinel', A. S. Viskov, and Y. N. Venevtsev, Resonance absorption of gamma quanta in barium, strontium, and calcium stannate, J. Exptl. Theoret. Phys. (U.S.S.R.) **44**, 1889 (1963) [J. Exp. Theor. Phys. **17**, 1271 (1963)].

[24] H. Micklitz and P. H. Barrett, Hyperfine interactions of ^{119}Sn atoms in rare-gas matrices at 4.2 K, Phys. Rev. B **5**, 1704 (1972).

[25] E. Fujita, S. Nasu, and Y. Yoshida, *Introduction to Mössbauer Spectroscopy: Its Principles and Applications* (AGNE Gijutsu Center, Tokyo, 1999), Chap. 1.

[26] A. A. Bahgat, Correlation between Einstein and Debye models of lattice vibrations for Mössbauer fraction, Phys. Status Solidi A **63**, K39 (1981).

[27] J. Bolz and F. Pobell, Mössbauer effect of ^{119}Sn in amorphous superconducting metals, Z. Phys. B **20**, 95 (1975).

[28] C. Hohenemser, Measurement of the Mössbauer recoilless fraction in β-Sn for 1.3 to 370°K, Phys. Rev. **139**, A185 (1965).

[29] A. Svane, N. E. Christensen, C. O. Rodriguez, and M. Methfessel, Calculations of hyperfine parameters in tin compounds, Phys. Rev. B **55**, 12572 (1997).

[30] R. Kurian and M. Filatov, Calibration of ^{119}Sn isomer shift using *ab initio* wave function methods, J. Chem. Phys. **130**, 124121 (2009).